Imaging and Localizing Interventional Devices by Susceptibility Mapping Using MRI

Ying Dong, *IEEE Member*, Zheng Chang, *IEEE Member,* and Jim Ji, *IEEE Senior Member*

***Abstract*— MRI has been used for imaging interventional procedures with devices such as brachytherapy seeds, biopsy needles, markers, and stents. However, the high susceptibility of these devices leads to signal loss and distortion in the MRI images. Previously, we proposed a method to generate positive contrast of the brachytherapy seeds using a regularized L_1 minimization algorithm. In this paper, we further developed and tested the method to image larger interventional devices based on susceptibility mapping. Computer simulations and experiments were performed using phantoms made of platinum wires and titanium needles. The results show that the proposed method provide positive contrast images of devices, therefore improves the visualization and localization of the devices.**

I. Introduction

Certain interventional procedures, such as brachytherapy, biopsy and angioplasty, can be monitored using MRI if the devices used are MRI compatible. However, the objects, such as needles, markers, stents, and brachytherapy seeds, usually have high magnetic susceptibility. The high-susceptibility objects will affect their surrounding area and introduce fast dephasing thus decrease the signal-to-noise ratio (SNR). The low magnitude can spread out to an area of several times larger than the devices itself creating dark spots in the MR images [1, 2]. This artifact hinders the accuracy of the localization of the devices, and prevents MRI from being widely used in these procedures.

To accurately locate the brachytherapy seeds, our group has previously proposed a method based on susceptibility mapping to provide the positive contrast seed images [3]. In the method, susceptibility is calculated by deconvoluting the magnetic field map with a dipole kernel. In this application, the devices are small (on the order of voxel size). However, with biopsy or angioplasty, the biopsy needles or stents have a much larger physical size and more severe signal loss. Susceptibility mapping of these devices has not been demonstrated due to the signal void or low SNR at or near the device locations.

Common methods to localize and provide positive-contrast of these devices includes shifting the surrounding data to the location of the devices [4], mapping the susceptibility gradient by selectively turn the negative contrast into a positive contrast using a filter or short-term Fourier transform [5, 6]. However, these methods depend on pre-knowledge of the susceptibility of the devices and provide limited resolution.

In this paper, we extend our previous method to image other highly susceptible objects, creating positive contrast images for localization of these devices. To test the proposed method, a gelatin phantom with a piece of platinum wire (susceptibility ~279ppm) and a water phantom with a titanium (susceptibility ~182ppm) biomarker needle are imaged and the corresponding positive contrast images are generated [7]. Results show that the proposed method can provide much improved visualization of devices in positive contrast and help to achieve better devices localization.

II. Theory and Method

The magnetic field due to a susceptible object can be characterize as a linear sum of the fields from it finite elements. Therefore, the local magnetic field $\Delta\mathbf{B}(\mathbf{r})$ can be modeled as the convolution of the spatial susceptibility distribution of the object(s) $\chi(\mathbf{r})$ and a dipole kernel [8].

$$\Delta\mathbf{B}(\mathbf{r}) = \boldsymbol{\kappa}(\mathbf{r}) \otimes \boldsymbol{\chi}(\mathbf{r}) \tag{1}$$

where $\boldsymbol{\kappa}(\mathbf{r})$ is the dipole kernel [9, 10]. $\Delta\mathbf{B}(\mathbf{r})$ can be measured using the phase image. In principle, the susceptibility distribution can be obtained by kernel deconvolution. However, the problem is ill-conditioned and thus a regularization is needed.

A. Susceptibility mapping using regularized L_1 minimization

L_1 regularization is imposed to calculate the susceptibility map $\boldsymbol{\chi}$ [9, 11, 12].

$$\min_{\boldsymbol{\chi},\lambda} f(\boldsymbol{\chi},\lambda) = \left\| \mathbf{W}(\boldsymbol{\kappa}\boldsymbol{\chi} - \Delta\mathbf{B}) \right\|_2^2 + \lambda \left\| \mathbf{M}\mathbf{G}\boldsymbol{\chi} \right\|_1 \tag{2}$$

where λ is a Lagrangian parameter, $\mathbf{W}$ is a weighting matrix, $\mathbf{M}$ is a masking matrix, and $\mathbf{G}$ is a first-order gradient operator. The introduction of $\mathbf{W}$ is to reduce the weights of the unreliable data at the immediate vicinity of the susceptible objects. $\mathbf{W}$ is achieved by normalizing the magnitude image. The introduction of $\mathbf{M}$ is to avoid over-smoothing of the small structure of the susceptible objects. $\mathbf{M}$ is achieved by thresholding the magnitude image. $\mathbf{M}$ eliminates the interventional devices and its immediate vicinity. However, $\mathbf{M}$ does not need to match the location of the highly susceptible objects. Some noisy area may also be masked out by $\mathbf{M}$, which will not affect the result of calculation.

Research supported by NSF.

Y. Dong is with the Department of Electrical and Computer Engineering, Texas A&M University, College Station, TX 77843-3128 USA (e-mail: dongying09@tamu.edu).

Z. Chang is with the Department of Radiation Oncology, Duke University, Durham, NC 27708 USA (e-mail: zheng.chang@duke.edu).

J. Ji is with the Department of Electrical and Computer Engineering, Texas A&M University, College Station, TX 77843-3128 USA (corresponding author: Jim Ji, phone: 979-458-1468; fax: 979-845-6259; e-mail: jimji@tamu.edu).

978-1-4244-7929-0/14/$26.00 ©2014 IEEE

Minimizing the first term can get the result loyal to the acquired data, whereas minimizing the second term can promote the sparsity and denoising. λ is used to balance the two terms.

Eq. 2 is similar to the equations in [10, 13, 14], however, the rational and definition of $\mathbf{M}$ is different. [10] assumes that the edge of the susceptibility objects and the edge of the magnitude images appear at the same location, which is not true in the application with high susceptible objects.

The solution to Eq. 2 is achieved by finding the zero point of its first-order derivative.

$$\frac{\partial f}{\partial \boldsymbol{\chi}} = 2\boldsymbol{\kappa}^H \mathbf{W}^H(\mathbf{W}(\boldsymbol{\kappa}\boldsymbol{\chi} - \Delta\mathbf{B})) + \lambda\nabla\left\|\mathbf{M}\mathbf{G}\boldsymbol{\chi}\right\|_1 = 0 \qquad (3)$$

where ^{H} is the conjugate transpose of the operator/matrix.

B. Measuring $\Delta\mathbf{B}$ map using a spin-echo sequence with a shifted 180° pulse

Unlike other susceptibility mapping method, the proposed method uses a spin-echo sequence instead of a gradient echo sequence. A well-known feature of the spin-echo sequence is that it can refocus the dephasing due to the field inhomogeneity (introduced by B_0 inhomogeneity and susceptibility) using a 180° pulse. Therefore, it is not suitable for susceptibility mapping method. However, we propose to use spin-echo sequence with a shifted 180° pulse, as shown in Fig. 1, where T_{shift} is defined as positive when the 180° pulse shifted towards the acquisition [15, 16]. This pulse sequence maintains the dephasing due to the field inhomogeneity and provides high SNR. Moreover, the amount of dephasing due to the susceptible objects is equivalent to that from an ultra-short gradient-echo sequence with $TE = -2T_{shift}$, whereas the latter imposes a high requirement on the gradient of the MR system. Therefore, the spin-echo sequence with a shifted 180° pulse is well suited and easy to achieve for the application of highly susceptible objects, because the rapid dephasing requires short TE to avoid phase wrapping.

C. Data simulations and experimental acquisitions

Two highly susceptible objects were imaged using a 4.7T Varian 33cm scanner. In the first experiment, a platinum wire was placed in a gelatin phantom. A spin-echo sequence with a shifted 180° RF pulse was applied. The matrix size was 128×128×9. The FOV was 70×70mm^2. The slice thickness was 1.5mm without slice gap. The TR was 2s, and the TE was 30ms. Six sets of images were acquired, with 180° RF pulse being shifted by T_{shift} =[0, 0.1, 0.2, 0.3, 0.4, 0.5]ms respectively. The scan time for each set of date is 4min 16s. Phase unwrapping was applied on the phase images. Two selected sets of data were used to calculate the field map, according to $\Delta\mathbf{B} = \frac{-\Delta\boldsymbol{\varphi}}{2\gamma B_0 \Delta T_{shift}}$, where $\Delta\boldsymbol{\varphi}$ is the phase change after phase unwrapping, and γ is the gyromagnetic ratio.

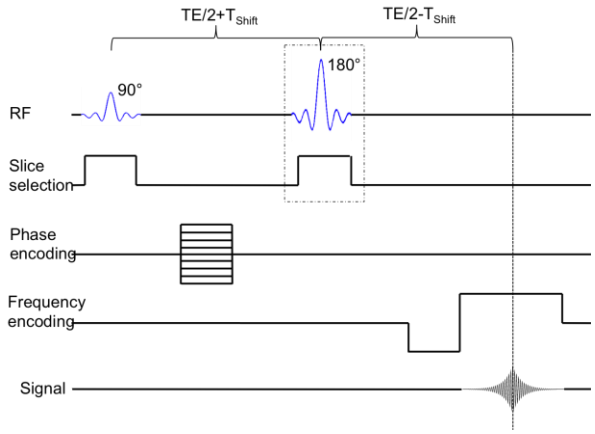

Fig.1 The diagram of the spin-echo sequence with a shifted 180° pulse.

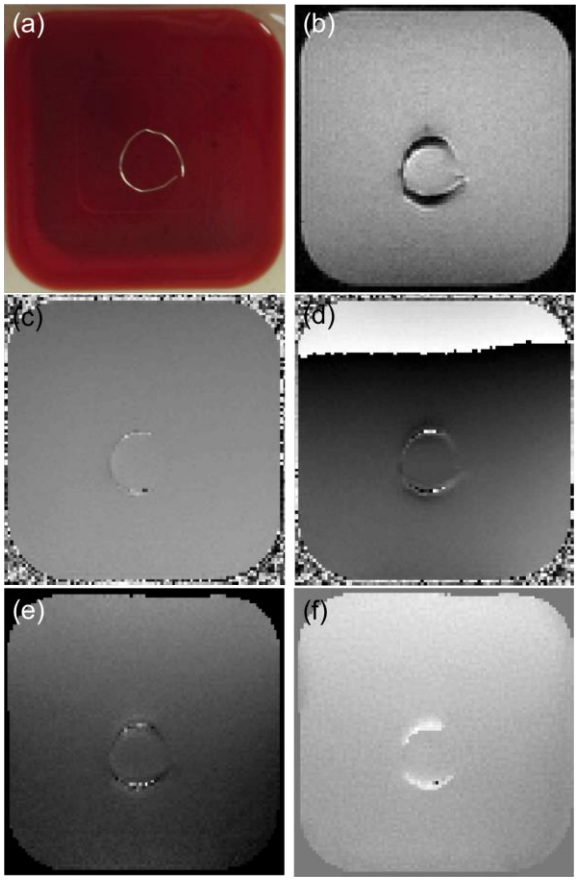

Fig.2 (a) Photo of the platinum wires in a gelatin phantom; (b) MR magnitude image; (c) phase image with T_{shift} = 0ms, (d) phase image with T_{shift} = 0.2ms; (e) calculated field map; and (f) susceptibility image from the proposed method. The edges of the images are cropped for better visualization.

A computer simulation was conducted to mimic the experimental setup and explore the accuracy of the susceptibility calculation. A high resolution images with 61um x 61um x 0.17mm resolution and 1152x1152x81 image size were created. Independent Gaussian noise was added to the real part and imaginary part of the data separately. Then the data was summated and averaged to

128x128x9 to simulate the spin-spin interaction. The other parameters were chosen so that they were consistent with the experimental data. The shape of the titanium wire was simplified as a circle.

In the second experiment, a biomarker needle was inserted in to a water phantom, which was doped with 1g/L copper sulfate. The acquisition parameters were the same as the first experiment.

This deconvolution reconstruction procedure was performed offline using Matlab (Math Works, Natick, MA) and a house-made nonlinear conjugate gradient method. The computer has 2.5GHz Intel Core i5, 4GB 1600 MHz DDR3 memory and OS X system. Multiple regularization parameters were tested and visually compared to choose the best results.

III. Results

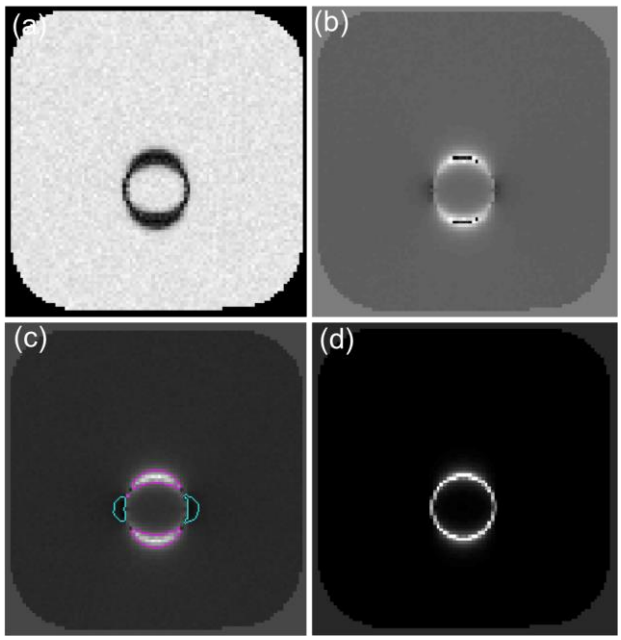

Fig.3 The results from the computer simulation. (a) Magnitude image; (b) Phase image when T_{shift} = 0.2ms; (c) the ideal field map without noise, with +/-10ppm contour labeled; and (d) the susceptibility map calculated using the proposed method.

Fig. 2 shows the results from the first phantom experiment. Fig. 2(a) shows the gelatin phantom with the platinum wires (more gelatins were later filled on top of the platinum wire). Fig. 2(b) shows a representative magnitude image in the center slice using the spin-echo sequence with a shifted 180º pulse. Because of the high susceptibility of the platinum, the magnitude image shows dark area up to 2.2mm in ring width, comparing with the diameter of the wire of 0.3mm. Fig. 2(c) and (d) shows the corresponding phase images when T_{shift} = 0ms and 0.2ms. When T_{shift} = 0ms, the phase should be uniform across the phantom. However, the field variation induced by the high susceptibility will affect the excitation pattern. To calculate the field map, different ΔT_{shift} are tested. ΔT_{shift} = 0.1ms can provide correct field map, as shown in Fig. 2(e). And Fig. 2(f) shows the susceptibility map calculated using the proposed method. Comparing to Fig. 2(b), the platinum wire shows in positive contrast in Fig. 2(f), making it much easier to see and localize.

Fig. 3 shows the results of the computer simulation. Fig. 3(a) and (b) show the magnitude and phase image (T_{shift} = 0.2ms) of the center slice in the simulation. They correspond well to Fig. 2(b) and (d). Fig. 3(c) shows the field map and the +/-10ppm contour of the field map. Fig. 3(d) shows the susceptibility map calculated using the proposed method. The proposed method produced a highly localized, clear representation of the position of the susceptible objects.

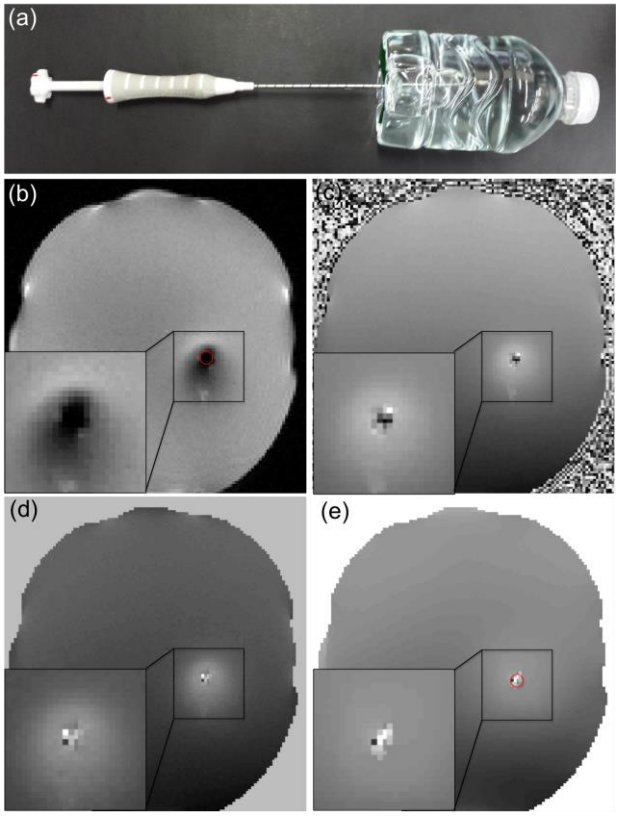

Fig.4 (a) Photo of the biomarker needle in water phantom; (b) magnitude image; (c) phase image with T_{shift} = 0.1ms; (d) field map calculated from the phase images; and (e) susceptibility map from the proposed method. The edges of the images are cropped for better visualization.

The results from the second phantom experiment are shown in Fig. 4. Fig. 4(a) shows a picture of the water phantom for the second experiment. The needle is made of titanium and the size of the needle is 14G (~2mm in diameter). The water is doped with copper sulfate to make the T_1 and T_2 of the water close to the human muscles. Fig. 4(b) and (c) shows the magnitude and phase (T_{shift} = 0.1ms) of the spin-echo sequence with a shifted 180º pulse, respectively. The presence of the needle introduces great distortion to both the magnitude and phase image. Fig. 4(d) shows the field map calculated from the phase images. And Fig. 4(e) shows the susceptibility map calculated using the proposed method. As shown, the susceptibility map

calculated using the proposed method reduces the image artifacts and shows the location in positive contrast.

IV. Discussion

The simulated and experimental results have clearly shown that the high susceptibility will introduce severe image distortion to the images. Therefore, for some procedures that require accurate location of the susceptible objects, such as brachytherapy, marker insertion and biopsy, the visual assistance provided by conventional MRI is limited. The proposed method can be used to reduce the location error in these procedures with MRI imaging.

The 180º pulse can recover the phase induced by the field inhomogeneity after the spins are tipped down to x-y plane. However, the strong field variation induced by the high susceptible devices is in the same order of that induced by the selection gradients. Therefore, there still is a little phase variation across the phantom for $T_{shift} = 0ms$, as shown in the result. To overcome this, a 3D spin-echo sequence should be applied. However, the 3D spin-echo sequence takes much longer time and thus not practical for clinical applications.

The scan time for each acquisition is about 4.5 min. In principle, only 2 acquisitions with two T_{shift} are required to do the calculation. That adds up to 9min. However, this only covers 9 slices that is 13.5mm for 1.5mm thickness. In clinical application, the acquisition time could be about 20 min ~ 30min for 50mm volume. During this time, the motion of the organ could result in inaccurate susceptibility map. A more time-efficient pulse sequence should be designed.

To correctly calculate the field map, the phase difference between the two consecutive T_{shift} cannot exceed 2π. Otherwise the phase unwrapping cannot correctly recover the phase change. This imposes a requirement on the ΔT_{shift} selection. The rapid phase wrap due to the high susceptibility will introduce error. Though no accurate phase of the pixel on and at the immediate vicinity of the highly susceptible objects is required for the calculation of the location. The study of T_{shift} selection will be one of our future researches.

V. Conclusion

In this paper, we presented a new method to image large, highly susceptible interventional devices by mapping their susceptibility using a regularized L_1 minimization. The feasibility of the proposed method was demonstrated using phantom experiments and simulations. To our best knowledge, this is the first time such mappings are done on large interventional devices. The potential of the method for providing positive-contrast device images instead of the conventional "black" or negative-contrast device images is very promising for interventional MRI. Recommended shift values in a spin-echo sequence were identified. Improved visualization and localization were achieved using the proposed method. The proposed method can help increase the accuracy of the interventional procedures.

Acknowledgement

This work was supported in part by the National Science Foundation under award number 0748180. Any opinions, findings and conclusions or recommendations expressed in this material are those of the authors and do not necessarily reflect those of the National Science Foundation.

References

[1] C. Ménard, R. C. Susil, P. Choyke, G. S. Gustafson, W. Kammerer, H. Ning, *et al.*, "MRI-guided HDR prostate brachytherapy in standard 1.5 T scanner," *Int J Radiat Oncol Biol Phys,* vol. 59, pp. 1414-1423, 2004.

[2] M. Stuber, W. D. Gilson, M. Schär, D. A. Kedziorek, L. V. Hofmann, S. Shah, *et al.*, "Positive contrast visualization of iron oxide - labeled stem cells using inversion - recovery with ON - resonant water suppression (IRON)," *Magn Reson Med,* vol. 58, pp. 1072-1077, 2007.

[3] D. Ying and J. Jim, "Positive contrast MRI of prostate brachytherapy seeds by susceptibility mapping," in *Engineering in Medicine and Biology Society (EMBC), 2012 Annual International Conference of the IEEE*, 2012, pp. 392-395.

[4] H. de Leeuw, P. Seevinck, and C. Bakker, "Center - out radial sampling with off - resonant reconstruction for efficient and accurate localization of punctate and elongated paramagnetic structures," *Magn Reson Med,* vol. 69, pp. 1611-1622, 2013.

[5] G. Varma, R. E. Clough, P. Acher, J. Sénégas, H. Dahnke, S. F. Keevil, *et al.*, "Positive visualization of implanted devices with susceptibility gradient mapping using the original resolution," *Magn Reson Med,* vol. 65, pp. 1483-1490, 2011.

[6] H. Dahnke, W. Liu, D. Herzka, J. A. Frank, and T. Schaeffter, "Susceptibility gradient mapping (SGM): A new postprocessing method for positive contrast generation applied to superparamagnetic iron oxide particle (SPIO) - labeled cells," *Magn Reson Med,* vol. 60, pp. 595-603, 2008.

[7] J. F. Schenck, "The role of magnetic susceptibility in magnetic resonance imaging: MRI magnetic compatibility of the first and second kinds," *Med Phys,* vol. 23, p. 815, 1996.

[8] J. D. Jackson and R. F. Fox, "Classical electrodynamics," *American Journal of Physics,* vol. 67, p. 841, 1999.

[9] J. Liu, T. Liu, L. de Rochefort, J. Ledoux, I. Khalidov, W. Chen, *et al.*, "Morphology enabled dipole inversion for quantitative susceptibility mapping using structural consistency between the magnitude image and the susceptibility map," *Neuroimage,* 2011.

[10] J. Liu, T. Liu, L. de Rochefort, J. Ledoux, I. Khalidov, W. Chen, *et al.*, "Morphology enabled dipole inversion for quantitative susceptibility mapping using structural consistency between the magnitude image and the susceptibility map," *Neuroimage,* vol. 59, pp. 2560-2568, 2012.

[11] M. Lustig, D. Donoho, and J. M. Pauly, "Sparse MRI: The application of compressed sensing for rapid MR imaging," *Magnetic Resonance in Medicine,* vol. 58, pp. 1182-1195, 2007.

[12] B. Kressler, L. de Rochefort, T. Liu, P. Spincemaille, Q. Jiang, and Y. Wang, "Nonlinear regularization for per voxel estimation of magnetic susceptibility distributions from MRI field maps," *Medical Imaging, IEEE Transactions on,* vol. 29, pp. 273-281, 2010.

[13] T. Liu, J. Liu, L. de Rochefort, P. Spincemaille, I. Khalidov, J. R. Ledoux, *et al.*, "Morphology enabled dipole inversion (MEDI) from a single - angle acquisition: Comparison with COSMOS in human brain imaging," *Magn Reson Med,* vol. 66, pp. 777-783, 2011.

[14] J. Li, S. Chang, T. Liu, Q. Wang, D. Cui, X. Chen, *et al.*, "Reducing the object orientation dependence of susceptibility effects in gradient echo MRI through quantitative susceptibility mapping," *Magn Reson Med,* vol. 68, pp. 1563-1569, 2012.

[15] J. Ma and F. W. Wehrli, "Method for image-based measurement of the reversible and irreversible contribution to the transverse-relaxation rate," *J Magn Reson,* vol. 111, pp. 61-69, 1996.

[16] D. A. Yablonskiy and E. M. Haacke, "An MRI method for measuring T2 in the presence of static and RF magnetic field inhomogeneities," *Magn Reson Imaging,* vol. 37, pp. 872-876, 1997.